Influence of the rigid alumina particles added to ZrO$_2$ ceramics stabilized with Y$_2$O$_3$ for its mechanical properties

Marek Boniecki[1], Przemysław Gołębiewski[1], Helena Węglarz[1], Anna Piątkowska[1], Magdalena Romaniec[1], Konrad Krzyżak[1]

The effect of the phase added to ZrO$_2$ ceramics on its mechanical properties, and in partcular on the fracture toughness, was examined using the example of Al$_2$O$_3$ - ZrO$_2$ composite where ZrO$_2$ was stabilized with 3 mol% of Y$_2$O$_3$. Composites of 20% wt. Al$_2$O$_3$ - 80 wt.% ZrO$_2$ with different size of corundum grain were made. Vickers indenter crack resistance tests showed an increase of 21% in the value of this parameter for the samples with Al$_2$O$_3$ grains of approx. 6.5 µm in comparison with pure ZrO$_2$ ceramics. On the basis of literature data and microscopic observations, authors present a thesis that this increase is caused by two factors, i.e. the increase of the phase transition range (from tetragonal to monoclinic phase) accompanying crack propagation and the effect of large Al$_2$O$_3$ grains as bridges fastening the fracture surfaces.

Key words: ZrO$_2$ ceramics stab. 3 mol. %Y$_2$O$_3$, ceramic additives with a large Young's modulus, Al$_2$O$_3$ grain sizes, fracture toughness, bending strength

Wpływ sztywnych korundowych cząstek dodawanych do ceramiki ZrO$_2$ stabilizowanej Y$_2$O$_3$ na jej właściwości mechaniczne

Wpływ fazy dodawanej do ceramiki ZrO$_2$ na jej właściwości mechaniczne w tym głównie na jej odporność na pękanie zbadano na przykładzie kompozytu Al$_2$O$_3$ – ZrO$_2$ gdzie ZrO$_2$ było stabilizowane 3% mol Y$_2$O$_3$. Wykonano kompozyty 20% wag. Al$_2$O$_3$ – 80% wag. ZrO$_2$ różniące się wielkością ziarna korundowego. Badania odporności na pękanie prowadzone metodą wgłębnika Vickersa wykazały wzrost wielkości tego parametru o 21% dla próbek z ziarnami Al$_2$O$_3$ o wielkości ok. 6,5 µm w porównaniu z czystą ceramiką ZrO$_2$. Na podstawie danych literaturowych oraz własnych obserwacji mikroskopowych postawiono tezę, że wzrost ten spowodowany jest przez dwa czynniki tj. zwiększenie się zakresu przemiany fazowej (z fazy tetragonalnej do jednoskośnej) towarzyszącej propagacji pęknięcia oraz działaniem dużych ziaren Al$_2$O$_3$ jako mostków spinających powstające powierzchnie przełamu.

Słowa kluczowe: ceramika ZrO$_2$ stab. 3% mol. Y$_2$O$_3$, dodatki ceramiczne o dużym module Younga, wielkość ziaren Al$_2$O$_3$, odporność na pękanie, wytrzymałość na zginanie

1. Introduction

In comparison with the most structural material such as steel, ceramic are characterised by lower density, significantly higher resistance to various corrosive factors, such as high temperature and abrasion. Ceramic elements can be used as cutting tools, crucibles for melting metals and glass, as tools for semiconductor production, catalyst carriers for removing pollutants from car exhausts, as parts for car engines, turbochargers, brake discs, etc. [1-2]. Ceramics are also used for biomedical purposes (prostheses) [3] as well as transparent ceramics for making laser bars, windows or lenses [4].

The main obstacle to the wide use of ceramics as a structural material is primarily its brittle fracture, which can cause unexpected destruction of the element made of the material resulting from the development of subcritical cracks caused by applied stress [5]. In order to increase the resistance to cracking, we can use additives e.g. in the form of metal particles [6], fibers [7], carbon nanotubes [8], graphene flakes [9-12] or ceramic particles with higher stiffness (larger Young's modulus) than the matrix [13-25].

The aim of the work was to obtain ZrO$_2$ based composites with a high fracture toughness resulting from the introduction of the rigid ceramic particles (particles with high Young's modulus) to the zirconia matrix (stabilized with 3 mol% Y$_2$O$_3$). To prezent the example of such particles, Al$_2$O$_3$ grains were selected and then added to the ZrO$_2$ matrix (20% by weight which corresponds to a volume content of 28%).

2. Work hypotheses and literature review

The following hypotheses will be proved in this work: The overall fracture toughness K_{Ic} of zirconia based

[1] *Łukasiewicz Research Network - Institute of Electronic Materials Technology*, 133 Wólczyńska Str., 01-919 Warsaw, Poland e-mail: marek.boniecki@itme.edu.pl

Tab. 1. K_{Ic} for 3Y-TZP from literature.
Tab. 1. K_{Ic} dla 3Y-TZP na podstawie literatury.

K_{Ic} (MPam$^{1/2}$)	4.4	7.6	2.5	5 ± 0.5 (MED)	5.05 ± 0.03 (MED) 5.97 ± 0.06 (PQ)	5.5 ± 0.2 (MED)
Ref.	[11]	[14]	[16]	[20]	[23]	[31]
Formula for calculation	Anstis [29]	Anstis [29]	Anstis [29]	Niihara [30]	Niihara [30]	Niihara [30]

Tab. 2. Some properties of ceramics added to 3Y-TZP. The properties of 3Y-TZP are presented for comparison. Data sources are given in square brackets.
Tab. 2. Niektóre właściwości faz ceramicznych dodawanych do 3Y-TZP. Dla porównania pokazano właściwości ceramiki 3Y-TZP. W nawiasach kwadratowych podane są źródła danych.

Material → Properties ↓	ZrO$_2$ matrix	Al$_2$O$_3$	SiC [34]	TiC [35]	WC	TiB$_2$
E (GPa)	205 ± 4 [31]	370 ± 14 [31]	410	450	700 [22]	560 [35]
α (10^{-6}/°C)	10 (300 - 2000 K) [16]	8.6 (300 - 1800 K) [33]	4.0	8.5	5.2 [22]	5 (300 - 800 K) 9 (950 - 2000 K) [16]
ρ (g/cm^3)	6.1 [26]	3.98 [33]	3.1	4.93	15.7 [18]	4.52 [35]
H (GPa)	13.8 [31]	15 [33]	28	28	26 [36]	26 [35]

where : E is a Young's modulus, α is a coefficient of thermal expansion (CTE), ρ is a density and H is a Vickers hardness.

composites with rigid ceramic particles can be expressed as:

$$K_{Ic} = K_0 + \Delta K_{IcT} + \Delta K_{IcD} + \Delta K_{IcB} + \Delta K_{IcO} \qquad (1)$$

where K_0 is the inherent matrix toughness, i.e. the zirconia matrix without or with negligible transformation toughening, ΔK_{IcT} is the transformation toughening contribution, ΔK_{IcD} is the toughening due to crack deflection caused mainly by the rigid ceramic particles, ΔK_{IcB} is the toughening due to crack bridging and ΔK_{IcO} is the toughening due to other mechanisms for example crack branching.

ZrO$_2$ can be found in three polymorphic forms [26]. The stable polymorph at low temperatures has monoclinic structure. In the medium temperature range the tetragonal phase occurs. In the area of maximum to melting temperatures (2983 K), a stable phase of regular fluorite structur can be observed. The transformation of the tetragonal phase to monoclinic leeds to the appearence of cracks generated by the stress which is associated with volume expansion of 3 - 5%. It was found that annealing at high temperatures (1273-1773 K) in the presence of some oxides to stabilize the tetragonal or regular ZrO$_2$. The examples of the commonly used stabilizing oxides are: CaO, MgO, CeO$_2$ or Y$_2$O$_3$ (the last one is the most often used). These oxides formed with ZrO$_2$ solid solution, where in place of zirconium ions oxide cations are embedded. The addition of the oxides to ZrO$_2$ lowers the temperature of polymorphic transformations, reduces the volume changes and blocks the transformation. The metastable

phases: regular or tetragonal are obtained. The last one has very good mechanical properties, ie. high bending strength and fracture toughness [27-28] which originate from the stress-induced transformation of the tetragonal phase to monoclinic in the stress field of propagating cracks, a phenomenon known as transformation toughening (ΔK_{IcT} in (1)).

In this work 3 mol% Y$_2$O$_3$ stabilized tetragonal ZrO$_2$ (3Y-TZP) is proposed to be the ceramic matrix. In Tab. 1 there are some values of fracture toughness K_{Ic} for 3Y-TZP found in literature. In this case $K_{Ic} = K_0 + \Delta K_{IcT0}$ (where ΔK_{IcT0} means ΔK_{IcT} in (1) for ZrO$_2$ matrix).

K_{Ic} was determined using surface cracks made by Vickers indentation. The values were obtained using different formulas. Value 2.5 MPam$^{1/2}$ in [16] can be accepted as K_0 because only very small amount of monoclinic ZrO$_2$ was revealed on the fracture surfaces (hence $\Delta K_{IcT0} \approx 0$). K_{Ic} in [20, 23, 31] was calculated by Niihara median (MED) and Palmqvist (PQ) equation.

The values of K_{Ic} in Tab.1 in comparison with the value for steel, which is a very popular structural material ($K_{Ic} \approx$ 40 MPam$^{1/2}$ [32]), are several times smaller. In order to increase K_{Ic} of 3Y-TZP it is suggested to introduce rigid ceramic particles. It should induce several toughening mechanisms such as: crack deflection, branching or bridging of crack surfaces and it can also increase the ΔK_{IcT} share, which is shown later in the text. As result we can observe a significant increase in the fracture toughness of the composites.

On the basis of literature data [13-25] some ceramic particles used for reinforcement of 3Y-TZP are shown in Tab. 2.

All the ceramics added to 3Y-TZP have bigger E and H but smaller α than ZrO$_2$. As a consequence the residual thermal stresses are generated in composites during the process of cooling from sintering to room temperature [16, 21-25]. There are tensile in 3Y-TZP and compressive stresses in the added particles. For example, for the 30 vol.% TiB$_2$ - 70 vol.% ZrO$_2$ composite [16], the tensile stress in the matrix was estimated to be 0.26 GPa. On the other hand, for composites 10 vol.% Al$_2$O$_3$ - 90 vol.% ZrO$_2$ and 10 vol.% WC - 90 vol.% ZrO$_2$ [21] the maximum tensile stress in the matrix was 1.02 and 1.56 GPa respectively, and compressive stress in Al$_2$O$_3$ and WC respectively 0.66 and 1.35 GPa. The calculations of residual tensile stress in the ZrO$_2$ matrix (using the expression from [37]) gave the value of 0.44 GPa. In these calculations data for ZrO$_2$ and Al$_2$O$_3$ from Tab. 2 but Poisson's ratio equals 0.3 and 0.22 respectively. The residual tensile stresses in 3Y-TZP enhance its transformability and therefore the transformation toughening (ΔK_{IcT} in Eq.(1)). The influence of the residual stresses on transformation toughness could be explained in the following way:

Tab. 3. Relative improvement of fracture toughness ΔK_{Ic} of 3Y--TZP as a result of the introduction of the rigid particles (based on literature).

Tab. 3. Wzrost odporności na pękanie ΔK_{Ic} ceramiki 3Y-TZP wskutek wprowadzania do niej cząstek metalicznych (na podstawie literatury).

Particle material	Content (vol.%)	Grain size of additives (μm)	ΔK_{Ic} (%)	remarks	Ref.
Al$_2$O$_3$	30	6.5	30		[13]
Al$_2$O$_3$	20	3.0	64		[14]
Al$_2$O$_3$	10	-	20		[21]
SiC	5	0.15	11		[24]
TiC	20	1.84	17		[25]
WC	30	0.13 ± 0.05	46	*	[17]
WC	20	2.0	26	*	[18]
WC	20	1.6 ± 0.6	104	*	[19]
WC	10	0.13 ± 0.6	111	*	[19]
WC	10	1.82	30		[20]
WC	10	0.12	70		[20]
WC	10	-	60		[21]
WC	32	1.49	43		[23]
TiB$_2$	20	1.5 – 2.0	23		[15]
TiB$_2$	30	1.5 – 2.0	76		[16]

Where: ΔK_{Ic} (%) = $\Delta K_{Ic}/(\Delta K_{IcT0})$, * - ZrO$_2$ in these articles was stabilized by 2.8% Y$_2$O$_3$.

In the presence of tensile residual stress σ_r, the critical stress σ_{cT} required to initiate the stress-induced transformation in the crack tip would be reduced to σ_{cT}^m:

$$\sigma_{cT}^m = \sigma_{cT} - \sigma_r . \qquad (2)$$

The reduction in critical stress would actually contribute to the development of a larger transformation zone h according to the formula proposed in [38]:

$$h \sim (\sigma_{cT}^m)^{-2} . \qquad (3)$$

The increased transformation zone size enhances the transformation toughening contribution [39]:

$$\Delta K_{IcT} \sim h^{1/2} \sim (\sigma_{cT}^m)^{-1}. \qquad (4)$$

Hence ΔK_{IcT} is usually bigger than ΔK_{IcT0} for zirconia matrix.

The presence of secondary rigid particles in zirconia based composites causes crack deflection toughening mechanism which, for example, for 30 vol.% TiB$_2$ content in [16] increase the fracture toughness of about 15%. It could also cause crack bridging toughening because the grains of the additives (Tab. 3) are usually larger than the 3Y-TZP grains (0.3 - 0.5 μm [16]) and they are under the compressive strength in matrix. In this situation they could play a role of the bridges connecting the surfaces of the crack behind the head of the propagating crack. Tab. 3 presents the literature data of improvement of fracture toughness for 3Y-TZP reinforced by introducing rigid particles of various ceramics.

In the case of the addition of Al$_2$O$_3$ [13-14], an increase of fracture toughness was a function of the grain size. The data in Tab. 3 refer to the largest grain sizes used in [13-14]. Bending strength of the composites is usually not worse than for matrix ceramics. It is above 1 GPa [16, 20-21, 23-25].

3. Experimental part

3.1. Preparation of samples

The starting materials in our experiments were: commercial powder ZrO$_2$ stab. 3 mol.% Y$_2$O$_3$ delivered by Tosoh labelled as TZ-3Y-E with a purity of about 99.9% and crystal sizes 40 nm and Sumitomo Al$_2$O$_3$ powders with a purity of 99.99% designated as AA-04 and AA-18 with different grain sizes was used as starting materials. A mixture of powders in a proportion of 20 wt.% Al$_2$O$_3$ and 80 wt.% ZrO$_2$ as well as pure ZrO$_2$ powder (for making the matrix) were placed in a planetary mill in a container of stabilized ZrO$_2$ with balls with a diameter of 5 mm made from above material. The deionized water together with the plasticizer (Dolapix CE64) was added to the powder in an amount allowing to obtain a slurry with a content of 75% by weight of dry matter, and then stirred for

one hour at a speed of 150 rpm. After adding the binder (Duramax B1000) the suspension was stirred for 30 min at 100 rpm. The granules prepared in this way were made using cryogenic granulation method. 65 × 40 × 8 mm shaped moldings were pressed from the granulates, which were densified with isostatic pressure of 120 MPa. The moldings were sintered in two stages: initially at 800ºC, then at 1480ºC for 2 h (in air). The sintered bodies were cut and ground into beams for measuring mechanical properties. Part of the beams was polished unilaterally.

3.2. Tests of mechanical properties

The aim of our work was to measure fracture toughness K_{Ic}, bending strength σ_c, Young's modulus E and Vickers hardness H were measured. K_{Ic} measurements were carried out using three methods:

(a) By three-point bending of notched beams:

The measurements were carried out on 2.5 mm × 4 mm × 30 mm beams. The beams were cut in the middle (along the side of a length of 4 mm) to a depth of 0.9 mm using a circular saw with a thickness of 0.2 mm, and then to a depth of 0.2 mm with a disk thickness of 0.025 mm. The distance of the L supports was 20 mm. The samples were loaded with a crosshead displacement speed of 1 mm/min. The K_{Ic} value was calculated from the formula:

$$K_{Ic} = Y \frac{1.5 P_c L}{b w^2} \; c_k^{0.5}, \tag{5}$$

where: Y - geometrical constant calculated according to [40], P_c - breaking load, $b = 2.5$ mm - beam width, $w = 4$ mm - beam height, c_k - notch length (about 1.1 mm)

(b) By measuring the bending strength of the sample with the previously introduced Vickers fracture.

The measurements were carried out on samples with the dimensions described in paragraph (a) with a polished surface of 4 mm × 30 mm. In the centre of the polished surface of the sample, a Vickers indent was made under the load of $P = 98.1$ N, so that one pair of cracks running from the corners was perpendicular to the edge of the sample. Four-point bending strength test was then performed with a crosshead displacement speed of 1 mm/min, placing the sample in such a way that the introduced crack was on the extended beam surface between the upper pressure rollers. The value of K_{Ic} was calculated from the following formula from [41]:

$$K_{Ic} = 0.59 (E/H)^{1/8} (\sigma_c P^{1/3})^{3/4}, \tag{6}$$

where: E - Young's modulus, H - Vickers hardness, $P = 98.1$ N - Vickers indenter load and σ_c - four-point bending strength calculated from formula (7):

$$\sigma_c = \frac{1.5 P_c (L - l)}{b w^2}, \tag{7}$$

where: P_c - breaking load, $L = 20$ mm - distance of lower supports, $l = 10$ mm - distance of upper pressure rollers, $b = 4$ mm - width, $w = 2.5$ mm - beam height.

c) K_{Ic} determined on the basis of measuring the length of cracks running from the corners of the Vickers impression.

The value of c, averaged from the measurements of the length of four cracks running from the tops of he indent, is introduced into the appropriate formula given in the literature. The most popular are the formulas given in [29-30]. According to [29]:

$$K_{Ic} = 0.016 \, (E/H)^{0.5} \, P/c^{1.5} \tag{8}$$

where: c - average length of Vickers cracks, the other parameters were defined earlier.

According to [30]:

$$K_{Ic} = \frac{0.129 H \sqrt{\alpha}}{\varphi} \left(\frac{E \varphi}{H} \right)^{0.4} \left(\frac{c}{\alpha} \right)^{-1.5} \tag{9}$$

where: a - half of the diagonal of a Vickers indent, $\varphi = 3$ [30]

K_{Ic} was determined by methods (a) and (b) as the average for 10 beams, In turn for method (c) of 10 Vickers indents measured on beams used subsequently in method (b).

Four-point bending strength σ_c was determined according to [42] with a crosshead displacement speed of 1 mm/min on samples with dimensions of 2 mm × 2.5 mm × 30 mm in the conditions described in point (b). The stretched surface (2.5 mm × 30 mm) was polished. Strength values were calculated from the formula (7) where b = 2.5 mm and w = 2 mm. The test was performed on 30 samples.

Young's E modulus was determined according to [43] by bending three-point beams with dimensions: 1 mm × 4 mm × 50 mm with the support distance $L = 40$ mm by registering the deflection value of the sample as a function of the applied stress P. The deflection values were recorded using an inductive sensor placed in the deflection arrow of the beam. The load was applied at a constant speed of 1 mm/min to $P_k < P_c$. The test was carried out on 10 samples. The value of E was determined from the formula:

$$E = \frac{L^3}{4 b w^3 C} \tag{10}$$

where: $b = 4$ mm, $w = 1$ mm, $C = \Delta y/\Delta P$ (the ratio of the increase in the deflection to the load increase)

All the measurements were made on the modernized Zwick 1446 machine supported by the testXpert III program.

Vickers indents were made on polished surfaces of the samples using a hardness tester equipped with a Vickers indenter. H values were calculated from the formula:

$$H = 1{,}8544 \, P/(2a)^2 \tag{11}$$

where: a – a half of the diagonal of Vickers' indent

3.3. Microscopic assessment of materials microstructure, fractures and cracks from Vickers indents

The microstructure of the samples was analysed on polished and etched sample surfaces. The samples were thermally etched at 1350°C in air for 0.5 h. Photographs of microstructures, notched bar cuts after K_{Ic} test (area close to the cutting face) and Vickers cracking were taken using the AURIGA CrossBeam Workstation scanning electron microscope (Carl Zeiss). The grain sizes were estimated using Feret's diameters by the Clemex Techn. Inc. image analysis program. The results were presented as mean and standard deviation, assuming that the grain sizes are normally distributed.
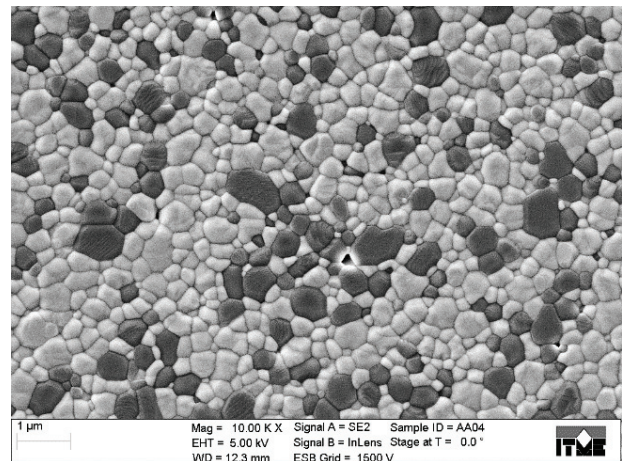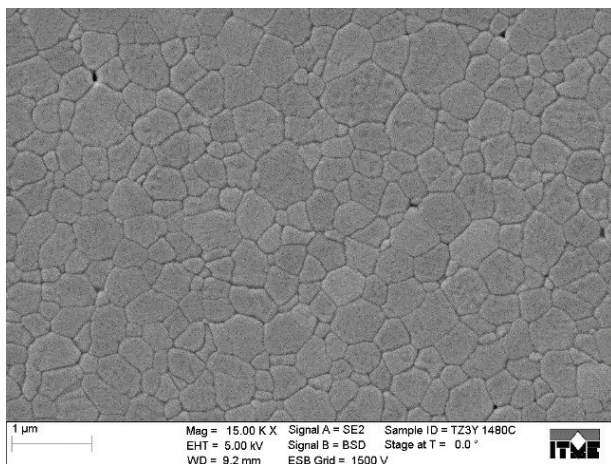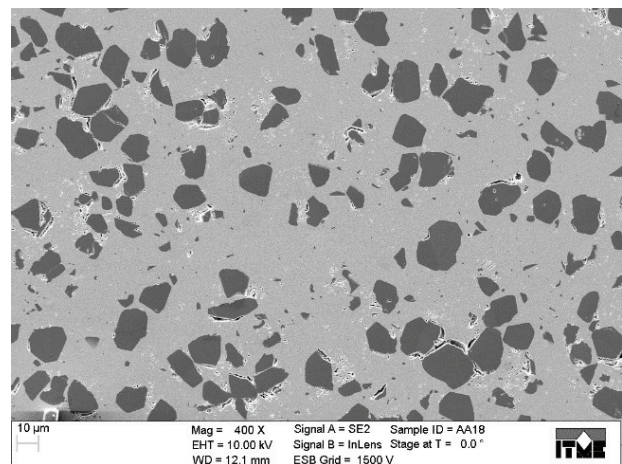

ZrO_2+AA-04

ZrO_2

ZrO_2+AA-18

Fig. 1. Microstructure of ZrO_2 samples and composites of 20% wt. Al_2O_3 - 80 wt.% ZrO_2. AA-04 and AA-18 indicated the Al_2O_3 powder types added to the ZrO_2 matrix. The bright grains are ZrO_2 and the dark ones are Al_2O_3.
Rys. 1. Mikrostruktura próbek tworzywa ZrO_2 oraz kompozytów 20% wag. Al_2O_3 – 80% wag. ZrO_2. AA-04 i AA-18 oznaczają rodzaje proszków Al_2O_3 dodane do matrycy ZrO_2. Jasne pola oznaczają ZrO_2, a ciemne Al_2O_3.

Table 4 presents the data characterizing the received materials.

Tab. 4. The size of grains D and relative density d of the obtained ceramic materials.
Tab. 4. Wielkości ziaren D oraz gęstości względne d otrzymanych tworzyw ceramicznych.

Material	$D_{Al_2O_3}$ (µm)	D_{ZrO_2} (µm)	d (%)
ZrO_2	-	0.41 ± 23	99.7
ZrO_2 + AA-04	0.31 ± 0.18	0.32 ± 0.18	99.8
ZrO_2 + AA-18	6.6 ± 4.1	0.21 ± 0.21	96.5
ZrO_2 + AA-18 1600	6.4 ± 3.2	0.55 ± 0.42	98.0

4. Results and discussion

Pictures of selected microstructures are shown in Fig.1.
Due to the relatively low density of ZrO_2 + AA-18, the additive samples were made from this composition, which were sintered at 1600°C for 2 hours.
In Table 5 the measured mechanical properties of the materials listed in Table 4 were collected, supplemented with ZrO_2 + AA-18 sintered at 1600ºC and 2 composites of 20% wt.%. Al_2O_3 - 80 wt.% ZrO_2 studied in other works.
Numbers in parentheses indicate the formulas from which K_{Ic} was calculated,
* Due to the lack of samples, this K_{Ic} composite was not determined by bending the notched or cracked beams introduced by the Vickers indenter nor as the bending strength or Young's modulus. The E value necessary to calculate K_{Ic} using formulas (8,9) was taken in the same way as for ZrO_2 + AA-18.

Material	K_{Ic} (MPam$^{1/2}$)				σ_c (MPa)	E (GPa)	H (GPa)
	(5)	(6)	(8)	(9)			
ZrO$_2$	5.45 ± 0.26	5.07 ± 0.08	3.73 ± 0.10	5.75 ± 0.16	888 ± 83	205 ± 4	13.8
ZrO$_2$ + AA-04	5.22 ± 0.37	4.73 ± 0.03	3.72 ± 0.20	5.44 ± 0.29	801 ± 203	242 ± 5	15.0
ZrO$_2$ + AA-18	5.26 ± 0.06	5.40 ± 0.09	4.11 ± 0.35	5.91 ± 0.50	517 ± 49	215 ± 6	11.6
ZrO$_2$ + AA-18 1600 *	-	-	4.52 ± 0.34	6.51 ± 0.49	-	-	11.6
ZrO$_2$ + TM-DAR OPUS 11 **	5.17 ± 0.31	4.51 ± 0.07	3.65 ± 0.16	5.33 ± 0.23	-	246 ± 8	15.0
ZrO$_2$ + Al$_2$O$_3$ Tosoh ***	5.46 ± 0.27	-	3.71 ± 0.18	-	1467 ± 262	235 ± 12	15.0

Tab. 5. Mechanical properties of ZrO$_2$ matrix and composites 20 wt.% Al$_2$O$_3$ - 80 wt.% ZrO$_2$.
Tab. 5. Właściwości mechaniczne matrycy ZrO$_2$ stabilizowanej 3% mol Y$_2$O$_3$ oraz kompozytów 20% wag. Al$_2$O$_3$ - 80% wag. ZrO$_2$.

** The composite was obtained while working on larger research project OPUS 11 No. 2016/21/B/ST8 /01027 implemented on 21/04/2017 in a scientific consortium, of which ITME is a member, and Lublin University of Technology is a leader. The material contains 20 wt.% Taimei corundum ceramics designated as TAIMICRON TM-DAR (the starting powder had a purity of 99.99% and a grain size of about 0.15 μm) and ZrO$_2$ stab. 3 mol% Y$_2$O$_3$ from Tosoh. The grain sizes determined on the polished and etched ceramic surface were 0.25 ± 0.07 and 0.22 ± 0.06 μm for Al$_2$O$_3$ and ZrO$_2$, respectively.

*** Our study concerning the composite was conducted within the framework of ITME statutory theme in 2016. The results were published in [44]. The implementation required a ready-made powder mixture of 20 wt.% Al$_2$O$_3$ and 80 wt.% ZrO$_2$ stab. 3 mol% Y$_2$O$_3$ with a purity of 99.9%, a crystallite the size of approx. 29 nm and granules of 60 μm provided by Tosoh. The grain sizes determined on the polished and etched ceramic surface were 0.41 ± 0.23 and 0.27 ± 0.17 μm for Al$_2$O$_3$ and ZrO$_2$, respectively. The high value of σc results from the use of very small test specimens (with a cross-section of 0.95 mm × 1mm × 12 mm at the distance of support of 8 mm).

Due to the low relative density of the ZrO$_2$ + AA-18 material and thus its relatively high porosity, there was a marked degradation of its mechanical properties (except for K_{Ic}) compared to ZrO$_2$ + AA-04. Sintering at a higher temperature (1600°C) improved the density and K_{Ic} of the composite with AA-18. The fracture toughness measured with the notched bar method calculated from (5) does not change as a function of the Al$_2$O$_3$ grain size, but it gets bigger for samples where the fracture was introduced by the Vickers indenter and when it was measured by the strength method and calculated from (6) and the cracks length was calculated from (8,9). Table 6 summarizes

Tab. 6. K_{Ic} calculated according to the formula (8) as a function of Al$_2$O$_3$ grain size of the tested materials.
Tab. 6. K_{Ic} obliczane wg wzoru (8) w funkcji wielkości ziarna Al$_2$O$_3$ badanych materiałów.

Materiał	$D_{Al_2O_3}$ (μm)	K_{Ic} (MPam$^{1/2}$)
ZrO$_2$	0	3.73 ± 0.10
ZrO$_2$ + TM-DAR OPUS 11	0.25 ± 0.07	3.65 ± 0.16
ZrO$_2$ + AA-04	0.31 ± 0.18	3.72 ± 0.20
ZrO$_2$ + Al$_2$O$_3$ Tosoh	0.41 ± 0.23	3.71 ± 0.18
ZrO$_2$ + AA-18	6.6 ± 4.1	4.11 ± 0.35
ZrO$_2$ + AA-18 1600	6.4 ± 3.2	4.52 ± 0.34

the values of K_{Ic} composites Al$_2$O$_3$ - ZrO$_2$ calculated from formula (8) in the function of the size of introduced Al$_2$O$_3$ grains (based on Tab. 4 and 5 and on the description under Tab. 5).

The increase in K_{Ic} for ZrO$_2$ + AA-18 1600 compared to ZrO$_2$ is around 21%. This result is similar to the one that obtained in [13], where the Al$_2$O$_3$ grain size was 6.5 μm and its volume content 30% and the increase in K_{Ic} by 30%. (in our case, the volume content of Al$_2$O$_3$ was 28%).

Fig. 2 shows the fracture surfaces of samples formed during the K_{Ic} study on notched beams.

It can be seen that cracks go through the grains of ZrO$_2$ and Al$_2$O$_3$. Photos of the cracks from the Vickers indents in Fig. 3 show that they pass through Al$_2$O$_3$ grains confirming fracture observations in Fig. 2.
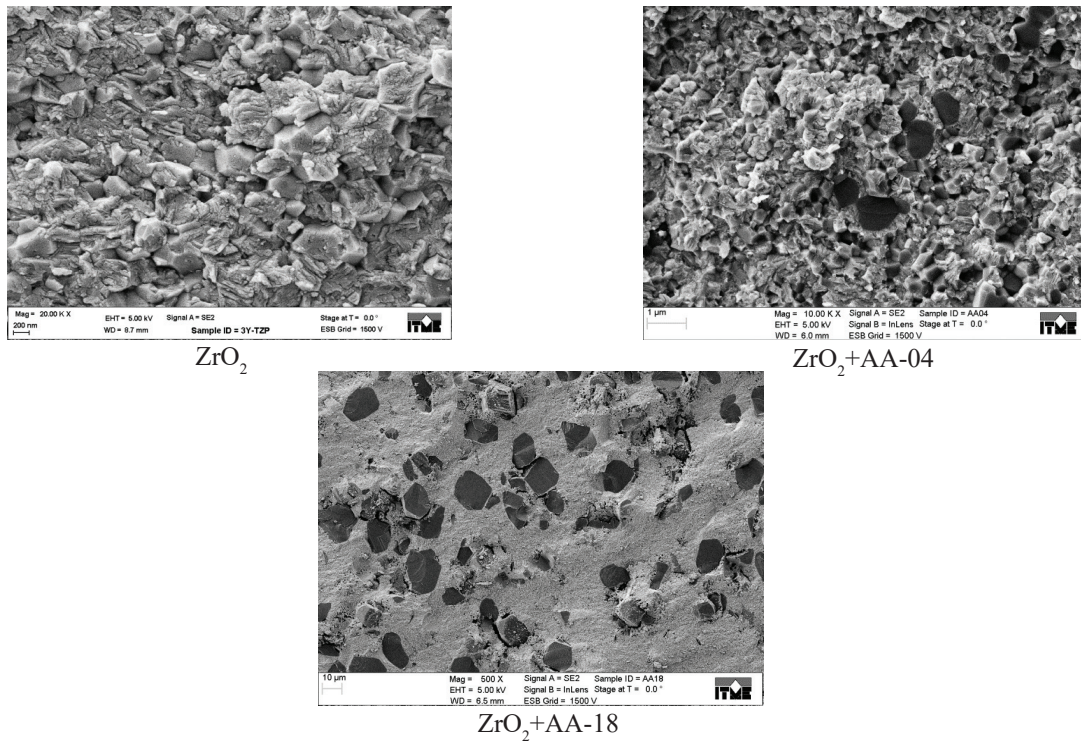
ZrO₂

ZrO₂+AA-04

ZrO₂+AA-18

Fig. 2. Fracture surfaces of samples of ZrO₂ matrix and composites of 20 wt.% Al₂O₃ - 80 wt.% ZrO₂. AA-04 and AA-18 mean the Al₂O₃ powder types added to the ZrO₂ matrix. The bright fields are ZrO₂ and the dark ones are Al₂O₃.
Rys. 2. Przełamy próbek tworzywa ZrO₂ oraz kompozytów 20% wag. Al₂O₃ – 80% wag. ZrO₂. AA-04 i AA-18 oznaczają rodzaje proszków Al₂O₃ dodane do matrycy ZrO₂. Jasne pola oznaczają ZrO₂, a ciemne Al₂O₃.
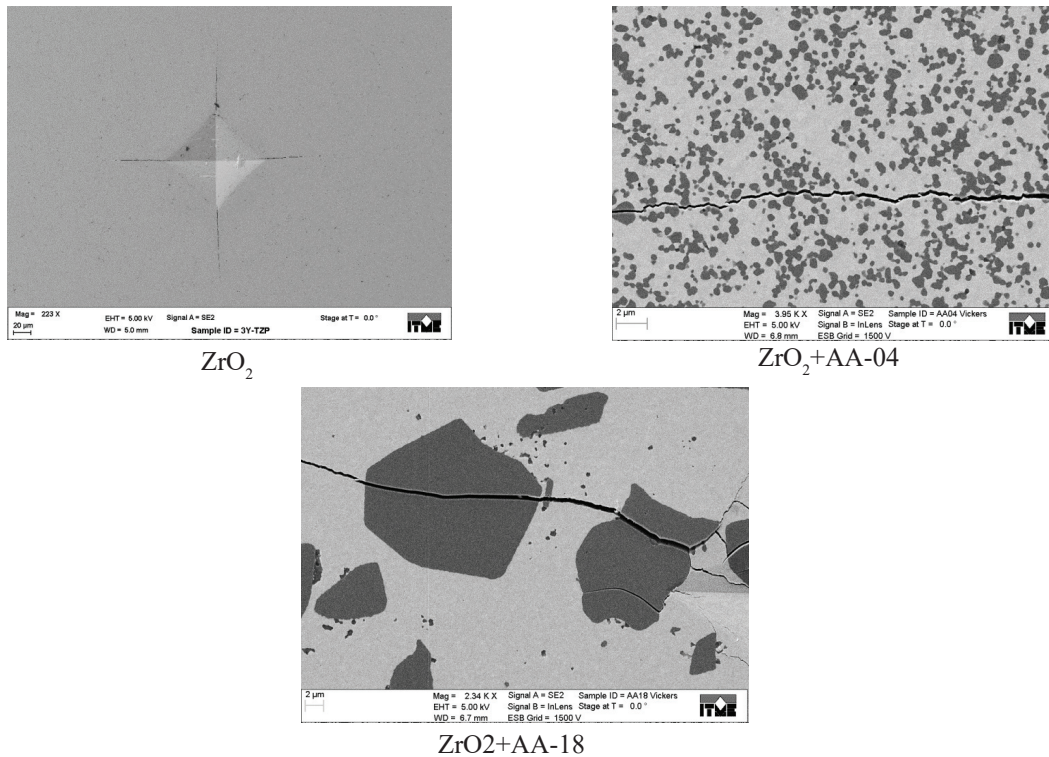

ZrO₂

ZrO₂+AA-04

ZrO2+AA-18

Fig. 3. Cracks from the Vickers indents in samples of ZrO₂ material and composites of 20 wt.% Al₂O₃ - 80 wt.% ZrO₂. The bright fields are ZrO₂ and the dark ones are Al₂O₃.
Rys. 3. Pęknięcia od odcisku Vickersa w próbkach tworzywa ZrO₂ oraz kompozytów 20% wag. Al₂O₃ – 80% wag. ZrO₂. Jasne pola oznaczają ZrO₂, a ciemne Al₂O₃.

The results presented in Tab. 5 and 6 and the microscopic observations in Fig. 2 and 3 are ambiguous. On the one hand, we can see the increase in the number of composites as a function of Al_2O_3 grain size (at least for measurements by the Vickers indenter method), but microscopic observations do not provide clear evidence of deflection of the propagating cracks by Al_2O_3 grains which could be a reason for strenghtening the crack resistance as it was suggested in [13,14]. The fracture toughness K_{Ic} of the composite can be described by Eq. (1).

According to [16] $K_0 = 2.5 \pm 0.1$ MPam$^{1/2}$ (calculated using Eq. (8) from the Vickers indents for $P = 98.1$ N), the basic component of the Eq.(1) is ΔK_{IcT}. Therefore, K_{Ic} should decrease as different materials are added to the matrix. If this is not the case, it means that there is either an increase of ΔK_{IcT} component in the matrix or another toughening mechanism. As indicated in [16,21] material with a coefficient of thermal expansion α smaller than the matrix added to ZrO_2 matrix causes the appearance of local stresses during the cooling of the composite from sintering to room temperature: tensile stress in the matrix and compressive stress in the material being added. For Al_2O_3 α is smaller than for ZrO_2 (Tab.2). In [21] in composite 10 vol.% Al_2O_3 − 90 vol.% ZrO_2 the maximum tensile stress estimated in the matrix was 1.02 GPa, and compressing stress in Al_2O_3 - 0.66 GPa. It was shown in part 2 (Eq. 2 - 4) that the addition of another phase to the matrix with smaller α increases the phase transformation contribution in strengthening the matrix K_{Ic}. There is still no answer to two questions:

1. why do we observe the growth of K_{Ic} (measured by the Vickers method) as a function of the grain size of Al_2O_3?

2. why do not we observe the above increase when using the notched bar method?

Ad. 1. As it can be seen in Fig. 1-3 in the ZrO_2 + AA-18 composite there are large (reaching up to a dozen micrometers) Al_2O_3 grains surrounded by a matrix with submicron grains, which, according to previous considerations, are subjected to compressive stress. These grains can act as bridges connecting the surfaces created in the cracking process. Under the influence of the tensile stress accompanying the propagation of the crack during the pressure of the Vickers indenter, these bridges get broken. The energy needed to destroy the bridges causes an increase in the share of ΔK_{IcB} in the equation (1), and thus the K_{Ic} value for the composite with large Al_2O_3 grains is also increased.

Ad. 2. The measurement procedure, which is the introduction of a precracking by using the sawing method, has a significant influence on the results. The incision at the end has a width of about 25 µm. Propagation of the crack from the face of the incision initiated by the applied external tensile stress begins with a defect resulting from the cutting process. What is important in this process of a crack initiation is the situation in the immediate vicinity of defect. As mentioned earlier it is accompanied by phase transformation. In the case of the composite with AA-04,

the fine corundum grains are distributed more densely and then the material near this defect can be considered a composite in which the increase of ΔK_{IcT} (described before) compensates for a 20% weight loss of ZrO_2. On the other hand, in the case of the composite with AA-18, large corundum grains are distributed less often and the material near this defect may be considered as ZrO_2; K_{Ic} values are similar to the values obtained for pure ceramics. Therefore for the three cases considered pure ZrO_2 and ZrO_2 with additions of AA-04 and AA-18, the similar K_{Ic} values are obtained within the error limits (Tab. 5).

5. Summary

This work presents the results of our study on the mechanical properties, and in particular the fracture toughness K_{Ic} of ZrO_2 ceramics stabilized with 3 mol% Y_2O_3 and composites with 20 wt.% Al_2O_3 - 80 wt.% ZrO_2. Two corundum powders of various grain sizes were used. Four materials: pure ZrO_2, composite with Al_2O_3 with grain size of approx. 0.3 µm and 2 composites with Al_2O_3 with a grain size of approx. 6.5 µm sintered at 1480 and 1600°C were obtained. An increase in K_{Ic} by 21% compared to a ZrO_2 matrix was found for a composite with a grain size of approx. 6.5 µm sintered at 1600°C. On the basis of literature data and our own microscopic observations, the thesis was made that this increase is caused by two factors: an increase in the phase transition range (from tetragonal to monoclinic phase) accompanying crack propagation as well as due to the operation of large Al_2O_3 grains asbridges fastening fracture surfaces.

Acknowledgments

References

[1] Okada A.: Automotive and industrial applications of structural ceramics in Japan, *J.Eur.Ceram.Soc.*, 2008, 28, 1097-1104.

[2] Okada A.: Ceramic technologies for automotive industry: Current status and perspectives, *Mater.Sci.Eng.B*, 2009, 161, 182-187.

[3] Manicone FP.F., Iommetti P.R., Raffaelli L.: An overview of zirconia ceramics: Basic properties and clinical applications, *J.of Dentistry*, 2007, 35, 819-826.

[4] Krell A., Hutzler T., Klimke J. : Transmission physics and consequences for materials selection, manufacturing, and applications, *J.Eur.Ceram.Soc.*, 2009, 29, 207-221.

[5] Wiederhorn S.M.: Subcritical crack growth in ceramics, in *Fracture Mechanics of Ceramics*, v.2 ed. By Bradt R.C., Hasselman D.P.H., Lange F.F., Plenum Press, New York, London, 1974, 613-646.

[6] Konopka K., Maj M., Kurzydłowski J.K.: Studies of the effect of metal particles on the fracture toughness of ceramic matrix composites, *Materials Characterization*, 2003, 51, 5, December, 335-340.

[7] Ostertag C.P.: Influence of fiber and grain bridging on crack profiles in SiC fiber-reinforced alumina-matrix composites, *Mater.Sci.Eng. A*, 1999, 260, 124-131.

[8] Bocanegra-Bernal M.H., Echeberia J., Ollo J.,et al.: A comparison of the effects of multi-wall and single-wall carbon nanotube additions on the properties of zirconia toughened alumina composites, *Carbon*, 2011, 49, 5, 1599-1607.

[9] Boniecki M., Gołębiewski P., Wesołowski W., et al.: Alumina/zirconia composites toughened by the addition of graphene flakes, *Ceram. Int.*, 2017, 43, 10066-10070.

[10] Liu J., Yan H., Reece M.J., Jiang K.: Toughening of zirconia/alumina composites by the addition of graphene platelets, *J.Eur.Ceram.Soc.*, 2012, 32, 4185-4193.

[11] Shin J-H., Hong S-H.: Fabrication and properties of reduced graphene oxide reinforced yttria-stabilized zirconia composite ceramics, *J.Eur.Ceram.Soc.*, 2014, 34, 1297-1302.

[12] Fei Ch., Jin D., Tyeb K., et al.: Field assisted sintering of graphene reinforced zirconia ceramics, *Ceram.Int.*, 2015, 41, 6113-6116.

[13] Li J-F., Watanabe R.: Fracture toughness of Al$_2$O$_3$ - particle-dispersed Y$_2$O$_3$ - partially stabilized zirconia, *J.Am.Ceram.Soc.*, 1995, 78, 1079-1082.

[14] Lee J-K., Kim M-J., Lee E-G.: Influence of dispersed-alumina particle size on the fracture toughness of 3 mol% yttria-stabilized zirconia polycrystals (3Y-TZP), *J.Mater.Sci.Lett.*, 2002, 21, 259-261.

[15] Vleugels J., Van der Biest O.: Development and characterization of Y$_2$O$_3$ – stabilized ZrO$_2$ (Y-TZP) composites with TiB$_2$, TiN, TiC, and TiC$_{0.5}$N$_{0.5}$, *J.Am.Ceram.Soc.*, 1999, 82 [10] 2717 – 2720.

[16] Basu B., Vleugels J., Van der Biest O.: Processing and mechanical properties of ZrO$_2$ – TiB$_2$ composites, *J.Eur.Ceram.Soc.*, 2005, 25, 3629-3637.

[17] Haberko K., Pędzich Z. Róg G., Bućko M.M., Faryna M.: The TZP matrix-WC particulate composites, *Eur.J.Solid State Inorg. Chem.*, 1995, 32, 593-601.

[18] Pędzich Z., Haberko K.: Toughening mechanism in the TZP - WC particulate composites, *Key Eng.Mater.*, 1997, 132-136, 2076-2079.

[19] Pędzich Z., Haberko K., Piekarczyk J., Faryna M., Lityńska L.: Zirconia matrix-tungsten carbide particulate composites manufactured by hot-pressing technique, *Mater. Lett.*, 1998, 70-75.

[20] Pędzich Z.: The reliability of particulate composites in the TZP/WC system, *J.Eur.Ceram.Soc.*, 2004, 24 3427-3430.

[21] Pędzich Z.: Fracture of oxide matrix composites with different phase arrangement, *Key Eng. Mater.*, 2009, 409, 244-251.

[22] Pędzich Z.: Tungsten Carbide as an reinforcement in structural oxide-matrix composites, *INTECH open science/open minds, chapter 4 (Tungsten Carbide - Processing and Applications)*, (2012), 81-102, (http://dx.doi.org/10.5772/51183).

[23] Űnal N., Kern F., Ővecoglu M.L., Gadow R.: Influence of WC particles on the microstructural and mechanical properties of 3 mol % Y$_2$O$_3$ stabilized ZrO2 matrix composites produced by hot pressing, *J.Eur.Ceram.Soc.*, 2011, 31, 2267- 2275.

[24] Bamba N., Choa Y-Ho, Sekino T., Niihara K.: Mechanical properties and microstructure for 3 mol% yttria doped zirconia/silicon carbide nanocomposites, *J.Eur.Ceram.Soc.*, 2003, 23, 773-780.

[25] Zhan G.-D., Lai T.-R., Shi J.-L., Yen T.-S., Zhou Y. Zhang Y.: Microstructure and mechanical properties of yttria-stabilized tetragonal zirconia polycrystals containing dispersed TiC particles, *J.Mater.Sci.*, 1996, 31, 2903-2907.

[26] Stevens R.: Zirconia and zirconia ceramics. Introduction to zirconia. Magnesium Electron Publication. 113, July (1986), 56 pages.

[27] Cutler R.A., Reynolds J.R., Jones A.: Sintering and characterization of polycrystalline monoclinic, tetragonal and cubic zirconia, *J.Am.Ceram.Soc.*, 1992, 73[8], 2173-2183.

[28] Govila R.K.: Strength characterization of yttria-partially stabilized zirconia, *J.Mater.Sci.*, 1995, 30, 2656-2667.

[29] Anstis G.R, Chantikul P., Lawn B.R., Marchall D.B.: A critical evaluation of indentation techniques for fracture toughness, *J.Am.Ceram.Soc.*, 1981, 64, 533-538.

[30] Niihara K.: A fracture mechanics analysis of indentation-induced Palmqvist crack in ceramics, *J.Mater. Sci. Lett.*, 1983, 2, 221-223.

[31] Boniecki M.: unpublished data, 2018.

[32] Bozkurt F., Schmidova E.: Fracture toughness evaluation of S355 steel using circumferentialy notched round bars, *Periodica Polytechnica Transportation Engineering*, 2018, 1-5, https://doi.org/10.3311/PPtr.11560.

[33] Munro R.G.: Evaluated material properties for a sintered α – alumina, *J.Am.Ceram.Soc.*, 1997, 80 (8), 1919-1928.

[34] https://accuratus.com/silicar.html.

[35] Vallauri D., Adrian I.C.A., Chrysanthou A.: TiC – TiB2 composites: A review of phase relationships, processing and properties, *J. Eur.Ceram. Soc.*, 2008, 28, 1697 – 1713.

[36] Małek O., Lauwers B., Perez Y., De Baets P., Vleugels J.: Processing of ultrafine ZrO_2 toughened WC composites, *J.Eur. Ceram.Soc.*, 2009, 29, 3371-3378.

[37] Selsing J.: Internal stresses in ceramics, *J.Am.Ceram. Soc.*, 1961, 44,419.

[38] Budiansky B., Hutchinson J.W., Lambropoulus J.C.: Continuum theory of dilatant transformation toughening in ceramics, *Int.J.Solids Struct.*, 1983, 19, 337-355.

[39] Evans A.G., Cannon R.M.: Toughening of brittle solids by martensitic transformation, *Acta Metall.*, 986, 34, 761-800.

[40] PN-EN ISO 15732, October 2007. Fine ceramics (advanced ceramics, advanced technical ceramics). Test method for fracture thoughness of monolithic ceramics at room temperature by single edge precracked beam (SEPB) method (ISO 15732:2003) (Eq. 8).

[41] Chantikul P., Anstis G.R., Lawn B.R, Marshall D.B.: A critical evaluation of indentation techniques for measuring fracture toughness: II, Strength method, *J.Am.Ceram.Soc.*, 1981, 64 [9], 539-543.

[42] PN – EN 843-1, December 2007. Advanced technical ceramics - Monolithic ceramics - Mechanical properties at room temperature - Part 1: Determination of flexural strength.

[43] PN-EN 843-2, December 2007. Advanced technical ceramics - Monolithic ceramics - Mechanical properties at room temperature - Part 2: Determination of the Young's modulus, shear modulus and Poisson's ratio.

[44] Boniecki M., Gołębiewski P., Wesołowski W. i inni: Kompozyt Al_2O_3-ZrO_2 wzmocniony płatkami grafenowymi/Al_2O_3-ZrO_2 composite reinforced with graphene platelets, *Materiały Elektroniczne/Electronic Materials*, 2016, 44, 1, 20-28.